SCIENCE CHINA
Information Sciences

• RESEARCH PAPER •

July 2021, Vol. 64 172213:1–172213:16
https://doi.org/10.1007/s11432-020-3128-2

Distributed event triggering control for six-rotor UAV systems with asymmetric time-varying output constraints

Liang CAO, Hongru REN*, Wei MENG, Hongyi LI & Renquan LU

Guangdong Province Key Laboratory of Intelligent Decision and Cooperative Control, Guangdong University of Technology, Guangzhou 510006*, China*

Received 16 June 2020/Revised 2 September 2020/Accepted 30 October 2020/Published online 20 May 2021

Abstract Inspired by the practical operability and safety of unmanned aerial vehicles (UAVs) in confined areas, this paper investigates adaptive trajectory tracking control problems in multiple six-rotor UAV systems with asymmetric time-varying output constraints and input saturation. Under model and disturbance uncertainties, six-rotor UAV systems are modeled as two non-strict-feedback systems, including attitude (inner-loop) and position (outer-loop) regulation systems. For the inner-loop design, the neural-based distributed adaptive attitude consensus control protocol is employed to realize the leader-follower consensus. Adaptive first-order sliding mode differentiators and an auxiliary dynamic system are introduced to address the "explosion of complexity" and saturation nonlinearity issues, respectively. Then, an event-triggered condition is predefined to alleviate the communication loads and reduce the number of messages to be transmitted from the controller to actuator. In addition, a class of asymmetric time-varying barrier Lyapunov functions are constructed for preventing the violation of time-varying output constraints. Accordingly, the proposed double-loop control strategies guarantee that all signals of UAV systems are semi-globally and uniformly bounded. Simulation results demonstrate that the proposed control method is effective.

Keywords adaptive neural control, asymmetric time-varying output constraints, event triggering mechanism, input saturation, six-rotor UAV systems

Citation Cao L, Ren H R, Meng W, et al. Distributed event triggering control for six-rotor UAV systems with asymmetric time-varying output constraints. Sci China Inf Sci, 2021, 64(7): 172213, https://doi.org/10.1007/s11432-020-3128-2

1 Introduction

In recent decades, the characteristics of unmanned aerial vehicle (UAV) systems, such as their vertical flight ability, hovering, smaller diameter, high agility, and maneuverability, have attracted increasing attention in many applications, including disaster monitoring, agricultural mapping, aerial cinematography, load transportation, rescue missions, and military surveillance [1–3].

However, UAV multi-rotor systems often suffer from various difficulties and challenges [4–6]. First, the multi-rotor dynamic model is known as the under-actuated system; i.e., the number of controllers is less than the number of degrees of freedom. Second, multi-rotor UAV systems are modeled as strong nonlinearity and coupling systems. Third, UAV systems often operate in complex environments, with wind disturbances, internal friction, aerodynamic damping forces, and constraints. With regard to the aforementioned issues, trajectory tracking control of multi-rotor UAV systems has received considerable attention [7–9]. For a four-rotor UAV with parametric uncertainties and external disturbances, a previous study [7] investigated the adaptive trajectory tracking control problem. Islam et al. [8] proposed a projection-based adaptive autonomous flight control scheme to improve the tracking accuracy of nonlinear four-rotor UAV systems with disturbances. As is known, the main advantages of multi-rotor UAV systems are their ability to hover, take off and land vertically, and fly in any direction. To solve the high-accuracy control problem of UAV systems with external disturbance force, the disturbance attenuation full tracking

* Corresponding author (email: renhongru2019@gdut.edu.cn)

control scheme was previously proposed in [10] to estimate external disturbances, where the position and attitude systems of the UAV were controlled effectively. It is worth noting that there has been an increasing interest in preserving the stability of attitude and position systems against disturbances and constraints. When multi-rotor UAV systems perform indoor fire-fighting, they are often required to fly within a limited or narrow space, where the range of the position is confined to a certain interval. The strong disturbances and high maneuverability of multi-rotor UAVs make it easier for them to transgress the boundary of constraints. Constraints are often divided into input saturation, output constraints, state constraints, error restriction, and physical stoppages [11–13]. Once the constraints are violated during operation, system performance may degrade or even lead to system damage. Some control methodologies have been previously presented [14–16] to prevent constraints violation. For example, to compensate for the input effects of dead zone and saturation, a bioinspired-model-based adaptive fuzzy sliding mode control method has been established [16], which is an effective and energy-efficient method. To analyze the convergence property of a multi-rotor UAV with output constraints, Zuo et al. [4] studied symmetric barrier Lyapunov functions (BLFs) with several quadratic terms. In the above-mentioned results, only static constraints are considered. However, complex missions often require the UAV to fly in time-varying space, where the physical environment confines the position, e.g., indoor fire-fighting and rescue missions. Therefore, investigating the problems of asymmetric time-varying output constraints is helpful in ensuring safe flight and obstacle avoidance. Tee et al. [17] adopted the asymmetric time-varying BLFs to prevent output constraint violation for strict-feedback nonlinear systems. Based on their results [17], Fu et al. [18] investigated the asymmetric time-varying output constraints of multi-rotor UAV systems with asymmetric time-varying BLFs, where they investigated the inner-loop control problem of strict-feedback nonlinear UAV systems.

Compared to an individual UAV system, multi-UAV systems can perform complicated missions efficiently, e.g., forest fire-fighting, load transportation, and military maneuvers. For the distributed cooperative control problem of multi-UAV systems, the main challenge is developing a distributed tracking control protocol with limited information interaction among UAV systems. For multi-UAV systems, some distributed control approaches have been reported [19–22]. In [19], a leader-follower structure and consensus-based algorithm were employed to propose the cooperative formation control schemes to address the problems related to collision-avoidance for a team of quad-rotor UAV systems. Dong et al. [20] presented the distributed formation containment protocols for achieving the desired formation of multi-UAV systems under directed topologies. Under a uniformly and jointly connected assumption and switching topologies, Zou et al. [21] proposed a distributed formation control scheme for a group of UAV systems. Unfortunately, only a few studies have investigated the limited communication resources for nonlinear multi-UAV systems.

To reduce the cost of multi-UAV systems, the small embedded micro-processor, onboard communication, and actuation modules are employed to transmit the communication information among agents, which limits both communication channel bandwidth and computation abilities [23–25]. To address the limited energy problem and computation and communication constraints in multi-agent systems, some triggering mechanisms have developed [26–32]. Based on the current sampled consensus error, a self-triggered consensus control protocol has been proposed [26] to reduce computation and communication costs of linear multi-agent systems. For second-order multi-agent systems with system nonlinearities, the distributed event-triggered sliding-mode control approach was presented [28] to effectively reduce state updates. In [30], a distributed event-triggered transmission mechanism was designed to reduce the amount of transmission data for heterogeneous multi-agent systems. However, problems related to consensus tracking control and the limited communication bandwidth of nonlinear multi-UAV systems with time-varying constraints have not been completely solved, which is the motivation of this study.

Inspired by the above observations and discussions, based on the event triggering technique, this paper concentrates on the adaptive consensus tracking control problem for nonlinear nonstrict-feedback UAV systems with asymmetric time-varying output constraints, input saturation and disturbance uncertainties. First-order sliding mode differentiator (SMD) is employed to handle the "explosion of complexity" problem caused by differentiating the virtual control signal repeatedly. In addition, a neural network (NN) is used to approximate unknown nonlinear functions of UAV systems and handle the algebraic loop problem. Then, adaptive backstepping NN control algorithms are presented to compensate for the effects of the model and disturbance uncertainties. An auxiliary function is introduced to effectively avoid the constraint of actuator input saturation. Finally, the good tracking accuracy of attitude and position systems is guaranteed, and all signals in the UAV systems are semi-globally uniformly ulti-

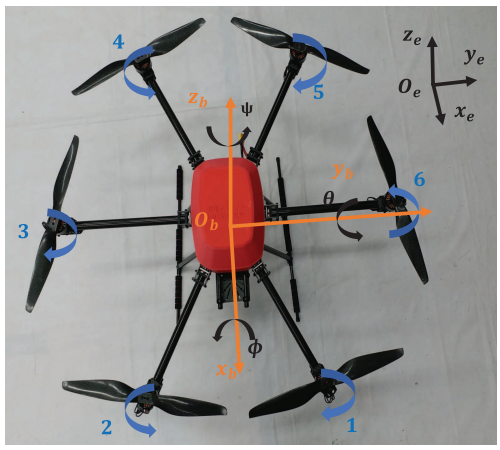

Figure 1 (Color online) Structure of the six-rotor UAV.

mately bounded (SGUUB). Our primary contributions are emphasized as follows. (i) If UAV systems have nonstrict-feedback forms, the aforementioned strategies will no longer be effective. In this paper, the nonstrict-feedback form is applied to describe UAV attitude and position systems, which is more general than the dynamic models of UAVs [5,6,10,18,33]. (ii) Unnecessary consumption of communication resources in limited channel bandwidth is reduced by the proposed event triggering control strategy. Compared to previously proposed event triggering mechanisms [25,28,30], the triggering mechanism presented in this paper reduces the release times of the controllers and avoids the unnecessary actuator wear. (iii) Differing from the static constraints [4,34], the asymmetric time-varying BLF is constructed to prevent the output from violating time-varying constraints of the nonlinear position system.

The remaining sections are arranged as below. In Section 2, the problem statement and some preliminaries are depicted. Then, the adaptive NN controller design and stability analysis are presented in Section 3. Furthermore, some simulation results are given to demonstrate the effectiveness of the proposed tracking control scheme in Section 4. Finally, the conclusion is drawn in Section 5.

2 Problem statement and preliminaries

2.1 Graph theory

A directed graph $\mathcal{G} = (\mathcal{V}, \mathcal{E})$ is employed to describe the information transmission among M subsystems, where $\mathcal{V} = \{1, \ldots, M\}$ stands for the nonempty set about nodes, $\mathcal{E} = \{(m, i) \subseteq \mathcal{V} \times \mathcal{V}\}$ represents the edge set. (m, i) indicates that the follower m can transmit the information to the follower i. The weighted adjacency matrix $\mathcal{A}$ is described as $\mathcal{A} = [a_{i,m}]_{M\times M}$, where the element $a_{i,i} = 0$. If and only if the pair $(m, i) \in \mathcal{E}$, $a_{i,m} > 0$, otherwise $a_{i,m} = 0$. The Laplacian matrix is defined as $\mathcal{L} = D - \mathcal{A}$ with the diagonal matrix $D = \mathrm{diag}\{\bar{d}_1, \ldots, \bar{d}_M\}$, and $\bar{d}_i = \sum_{m=1}^{M} a_{i,m}$. It is assumed that the digraph $\mathcal{G}$ has a spanning tree and the root node is the leader [35–39].

2.2 Model of six-rotor UAVs

In Figure 1, $\mathcal{E}_e = \{O_e, x_e, y_e, z_e\}$ and $\mathcal{B}_b = \{O_b, x_b, y_b, z_b\}$ denote the earth-fixed internal frame and body-fixed frame, where the center of mass of the multi-rotor is regarded as the origin, respectively. In frame $\mathcal{E}_e$, $\Theta = [\phi, \theta, \psi]^{\mathrm{T}}$ stands for the Euler angles (i.e., 'roll', 'pitch', 'yaw'), (x, y, z) is the coordinate of centroid. $\Omega = [\omega_x, \omega_y, \omega_z]^{\mathrm{T}}$ is the angular velocity in frame $\mathcal{B}_b$.

Considering the aerodynamic uncertainty, the model of UAV is constructed as

$$\begin{aligned} &\dot{\mathcal{P}} = \mathcal{V}, \quad \dot{\mathcal{V}} = \frac{1}{m}\mathcal{F}\mathcal{R}e_3 - ge_3 - \frac{\mathcal{K}\mathcal{V}}{m}, \\ &\dot{\Theta} = \mathcal{T}\Omega, \quad \mathcal{J}\dot{\Omega} = -\Omega \times (\mathcal{J}\Omega) + M - G_a + \mathcal{D}, \end{aligned} \tag{1}$$

where $\mathcal{P} = [x, y, z]^{\mathrm{T}} \in \mathbb{R}^3$ and $\mathcal{V} = [v_x, v_y, v_z]^{\mathrm{T}} \in \mathbb{R}^3$ denote the position vector and the velocity vector of the center of mass in $\mathcal{E}_e$, respectively. m stands for the total mass. g is the gravitational acceleration.

$\mathcal{J} = \mathrm{diag}\{J_x, J_y, J_z\}$ denotes the inertia matrix. $\mathcal{F}$ is the total thrust. $e_3 = (0,0,1)^{\mathrm{T}}$ is the unit vector. $M = [M_\phi, M_\theta, M_\psi]^{\mathrm{T}} \in \mathbb{R}^3$ is the total torque. Let $G_a = J_r(\Omega \times e_3)(\sum_{r=2,4,6}\Omega_r - \sum_{r=1,3,5}\Omega_r)$ denote the gyroscopic torque, where $\mathcal{J}_r$ is the rotor inertia, Ω_r stands for the angular velocity of rotor r. $\mathcal{K} = \mathrm{diag}(k_1, k_2, k_3)$ is an unknown diagonal aerodynamic matrix, where k_1, k_2, and k_3 stand for air drag coefficients. $\mathcal{D}$ is the disturbance described in $\mathcal{B}_b$, where $\mathcal{D} = \mathrm{diag}(d_\phi, d_\theta, d_\psi)\dot{\Theta}$. The rotation matrix $\mathcal{R}$ is expressed as

$$\mathcal{R} = \begin{bmatrix} C_\psi C_\theta & C_\psi S_\theta S_\phi - S_\psi C_\phi & S_\psi S_\phi + C_\psi S_\theta C_\phi \\ S_\psi C_\theta & C_\psi C_\phi + S_\psi S_\theta S_\phi & S_\psi S_\theta C_\phi - C_\psi S_\phi \\ -S_\theta & C_\theta S_\phi & C_\theta C_\phi \end{bmatrix},$$

where $C_{(\cdot)}$ and $S_{(\cdot)}$ stand for $\cos(\cdot)$ and $\sin(\cdot)$, respectively.

The transformation matrix $\mathcal{T}$ represents the relationship between $\mathcal{E}_e$ and $\mathcal{B}_b$, expressed as

$$\mathcal{T} = \begin{bmatrix} 1 & \sin\phi\tan\theta & \cos\phi\tan\theta \\ 0 & \cos\phi & -\sin\phi \\ 0 & \sin\phi\sec\theta & \cos\phi\sec\theta \end{bmatrix}.$$

Then, the attitude system is rewritten as

$$\begin{aligned} \ddot{\phi} =& -\dot{\theta}\dot{\psi}\frac{J_z - J_y}{J_x} + \frac{1}{J_x}(M_\phi - J_r\dot{\theta}\bar{\Omega} + d_\phi\dot{\phi}), \\ \ddot{\theta} =& -\dot{\phi}\dot{\psi}\frac{J_x - J_z}{J_y} + \frac{1}{J_y}(M_\theta - J_r\dot{\phi}\bar{\Omega} + d_\theta\dot{\theta}), \\ \ddot{\psi} =& -\dot{\phi}\dot{\theta}\frac{J_y - J_x}{J_z} + \frac{1}{J_z}(M_\psi + d_\psi\dot{\psi}), \end{aligned} \tag{2}$$

where $\bar{\Omega} = \Omega_2 - \Omega_1 + \Omega_4 - \Omega_3 + \Omega_6 - \Omega_5$.

And the position system can be presented as

$$\begin{aligned} \ddot{x} =& \frac{1}{m}(\cos\psi\sin\theta\cos\phi + \sin\psi\sin\phi)U_1 - \frac{k_1}{m}\dot{x}, \\ \ddot{y} =& \frac{1}{m}(\sin\psi\sin\theta\cos\phi - \cos\psi\sin\phi)U_1 - \frac{k_2}{m}\dot{y}, \\ \ddot{z} =& \frac{1}{m}(\cos\theta\cos\phi)U_1 - g - \frac{k_3}{m}\dot{z}, \end{aligned} \tag{3}$$

where $U_1 = F_1 + F_2 + F_3 + F_4 + F_5 + F_6$ denotes the force generated by the propellers with $F_r = b\Omega_r^2$ where b and Ω_r are the lift constant and rotary speed rotors, respectively.

In a UAV system, $U = [U_1, U_2, U_3, U_4]^{\mathrm{T}}$, $U_1 = \sum_{r=1}^{6} b\Omega_r^2$, $U_2 = bL(\Omega_6^2 - \Omega_3^2 + \sin(\pi/6)(\Omega_1^2 + \Omega_5^2 - \Omega_2^2 - \Omega_4^2))$, $U_3 = bL\sin(\pi/3)(\Omega_4^2 + \Omega_5^2 - \Omega_1^2 - \Omega_2^2)$, $U_4 = \upsilon(\Omega_1^2 - \Omega_2^2 + \Omega_3^2 - \Omega_4^2 + \Omega_5^2 - \Omega_6^2)$. U_2, U_3, and U_4 are defined as the roll input, pitch input and yaw input, respectively. L represents the distance from the center of rotor to the center of mass of the body. υ denotes the drag coefficient.

Remark 1. Compared with the quad-rotor UAV systems, the main characteristics of six-rotor UAV systems are the enhanced stability in the windy, hardware redundancy, payload capacity, and fault tolerance. In addition, the six rotors and propellers are distributed on both sides of the fuselage symmetrically [18]. Thus, considering the under-actuated, strong coupling characteristics and wind disturbances of six-rotor UAV systems, it is more difficult to construct the model.

2.3 Preliminaries

Lemma 1 ([40–42])**.** For the NN node number $l > 0$, any continuous function $\Re_{nn}(x)$ over a compact set $\Xi_i \subset \mathbb{R}^i$ can be approximated by $\theta^{*\mathrm{T}}\varphi(x)$. Then, one obtains

$$\Re_{nn}(x) = \theta^{*\mathrm{T}}\varphi(x) + \epsilon(x), \quad \forall x \in \Xi_i,$$

where θ^* means the ideal weight vector and $\varphi(x) = [\varphi_1(x), \ldots, \varphi_{\mathcal{N}}(x)]^{\mathrm{T}} \in \mathbb{R}^{\mathbb{N}}$ is the basis function. The approximation error $\epsilon(x)$ satisfies $|\epsilon(x)| \leqslant \epsilon^*$ with ϵ^* being an unknown constant.

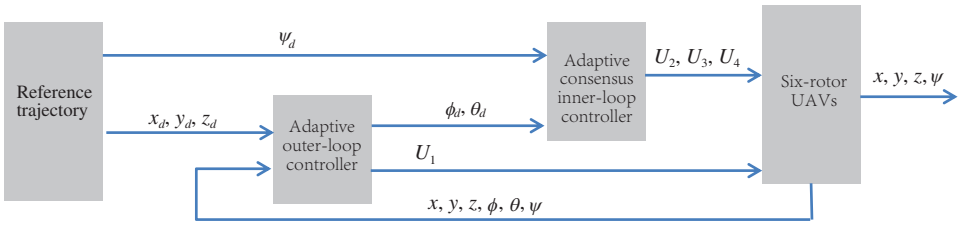

Figure 2 (Color online) Diagram of the control structure for six-rotor UAVs.

Lemma 2 ([43]). Let $\bar{x}_{i,a} = [x_{i,1}, \ldots, x_{i,a}]^{\mathrm{T}}$, and $\varphi_i(\bar{x}_{i,a}) = [\varphi_{i,1}(\bar{x}_{i,a}), \ldots, \varphi_{i,l}(\bar{x}_{i,a})]^{\mathrm{T}}$ stands for the basis function vector of NNs. For any positive constants a, b, if $b \leqslant a$, one has

$$\|\varphi_i(\bar{x}_{i,a})\|^2 \leqslant \|\varphi_i(\bar{x}_{i,b})\|^2. \tag{4}$$

Lemma 3 ([34]). Design the first-order SMD as follows:

$$\begin{aligned} \dot{\zeta}_{i,0} &= \eta_{i,0} = \zeta_{i,1} - \varepsilon_{i,0} \left|\zeta_{i,0} - \alpha_i(t)\right|^{1/2} \operatorname{sign}\left(\zeta_{i,0} - \alpha_i(t)\right), \\ \dot{\zeta}_{i,1} &= -\varepsilon_{i,1} \operatorname{sign}\left(\zeta_{i,1} - \eta_{i,0}\right), \end{aligned} \tag{5}$$

where $\zeta_{i,0}$, $\zeta_{i,1}$, $\eta_{i,0}$ stand for the states in system (5). $\varepsilon_{i,0}$ and $\varepsilon_{i,1}$ denote the first-order SMD parameters. $\alpha_i(t)$ is given as a known function. Moreover, the differential term $\dot{\alpha}_i(t)$ can be approximated by $\eta_{i,0}$ to arbitrary accuracy if the initial deviations $\zeta_{i,0} - \alpha_i(t_0)$ and $\eta_{i,0} - \dot{\alpha}_i(t)$ are bounded.

Assumption 1 ([4]). The Euler angles $\phi_i, \theta_i, \varphi_i$ of UAV satisfy the following condition: $\phi_i \in (-\frac{\pi}{2}, \frac{\pi}{2})$, $\theta_i \in (-\frac{\pi}{2}, \frac{\pi}{2})$, $\psi_i \in (-\pi, \pi)$.

Assumption 2 ([29]). External disturbances d_i, $i = 1, 2, \ldots, M$ satisfy $|d_i| < d_i^*$, where d_i^* denotes an unknown constant. The reference signal $y_{q0}(t)$ and its derivative $\dot{y}_{q0}(t)$ are bounded and smooth functions.

Assumption 3 ([17]). The system output y_n is bounded as $\underline{k}_{cn,1} < y_n < \bar{k}_{cn,1}$, where $\underline{k}_{cn,1}, \bar{k}_{cn,1}$ are the time-varying constraints. And $|\underline{k}_{cn,1}| \leqslant k_{c0}, |\bar{k}_{cn,1}| \leqslant k_{c1}, |\dot{\underline{k}}_{cn,1}| \leqslant k_{c2}$ and $|\dot{\bar{k}}_{cn,1}| \leqslant k_{c3}$ with k_{c0}, k_{c1}, k_{c2}, and k_{c3} being positive constants.

Lemma 4 ([17]). For $s \in \mathbb{R}$, positive constant $k_a \in \mathbb{R}^+$ and $|s| < k_a$, the inequality $\log \frac{k_a^2}{k_a^2 - s^2} \leqslant \frac{s^2}{k_a^2 - s^2}$ holds.

Remark 2. Different from the dynamic surface control (DSC) methods [14,18,27,32], with the characteristic of fast convergence and the good filtering precision, the first-order SMD is introduced to estimate the derivatives of virtual control signal in this paper. In addition, it is unnecessary to consider the partial derivative terms for the constructed SMD, which reduces the tedious analytic computation.

3 Design of adaptive NN controller

Firstly, an adaptive NN consensus tracking control strategy for the inner-loop system is proposed in Subsection 3.1. Then, the adaptive outer-loop control problem is solved in Subsection 3.2. Diagram of the control structure for six-rotor UAVs is presented in Figure 2.

3.1 Design of adaptive inner-loop controller

Taking the system (2) and disturbance uncertainties into account, the attitude system with three channels is expressed as

$$\dot{x}_{i,q1} = x_{i,q2} + f_{i,q1}(\bar{x}_{i,q2}), \quad \dot{x}_{i,q2} = u_{i,q}(\vartheta_{i,q}) + f_{i,q2}(\bar{x}_{i,q2}) + d_{i,q}, \quad y_{i,q} = x_{i,q1}, \quad q = 1, 2, 3, \tag{6}$$

where $x_{i,q1}$ and $x_{i,q2}$ stand for the states of the attitude system, where $x_{i,11} = \phi_i, x_{i,21} = \theta_i, x_{i,31} = \psi_i$, $x_{i,12} = \omega_{xi}, x_{i,22} = \omega_{yi}, x_{i,32} = \omega_{zi}$. $\bar{x}_{i,q2} = [x_{i,q1}, x_{i,q2}]^{\mathrm{T}}, i = 1, \ldots, M$. $f_{i,q1}(\bar{x}_{i,q2})$ and $f_{i,q2}(\bar{x}_{i,q2})$ stand for the neglected and unmodeled parts of the attitude system. $d_{i,1} = d_{\phi,i}\dot{\phi}_i + \dot{\theta}_i\dot{\psi}_i \frac{J_{y,i} - J_{z,i}}{J_{x,i}} - \frac{J_{r,i}}{J_{x,i}}\dot{\theta}_i\bar{\Omega}_i$,

$d_{i,2} = d_{\theta,i}\dot{\theta}_i+\dot{\phi}_i\dot{\psi}_i\frac{J_{z,i}-J_{x,i}}{J_{y,i}} - \frac{J_{r,i}}{J_{y,i}}\dot{\phi}\bar{\Omega}$, $d_{i,3} = d_{\psi,i}\dot{\psi}_i+\dot{\phi}_i\dot{\theta}_i\frac{J_{x,i}-J_{y,i}}{J_{z,i}}$. $u_{i,1}(\vartheta_{i,1}) = \frac{U_{i,2}}{J_{x,i}}$, $u_{i,2}(\vartheta_{i,2}) = \frac{U_{i,3}}{J_{y,i}}$, $u_{i,3}(\vartheta_{i,3}) = \frac{U_{i,4}}{J_{z,i}}$ mean the plant inputs subject to saturation nonlinearity, which are represented by

$$u_{i,q}(\vartheta_{i,q}) = \mathrm{sat}(\vartheta_{i,q}) = \begin{cases} \mathrm{sign}(\vartheta_{i,q}(t))u_{i,qN}, & |\vartheta_{i,q}(t)| \geqslant u_{i,qN}, \\ \vartheta_{i,q}(t), & |\vartheta_{i,q}(t)| < u_{i,qN}, \end{cases}$$

where $u_{i,qN}$ is the bound of $u_{i,q}(\vartheta_{i,q})$, $q = 1, 2, 3$.

A smooth function is defined to approximate the saturation function. That is, $\mathrm{sat}(\vartheta_{i,q})$ can be written as $\mathrm{sat}(\vartheta_{i,q}) = \varrho_{i,q}(\vartheta_{i,q}(t)) + \varsigma_{i,q}(\vartheta_{i,q}(t)) = u_{i,qN} \times \tanh(\frac{\vartheta_i}{u_{i,qN}}) + \varsigma_{i,q}(\vartheta_{i,q}(t))$, where $\varsigma_{i,q}(\vartheta_{i,q}(t)) = \mathrm{sat}(\vartheta_{i,q}) - \varrho_{i,q}(\vartheta_{i,q}(t))$ is a bounded function in time and its bound is expressed as

$$|\varsigma_{i,q}(\vartheta_{i,q}(t))| = |\mathrm{sat}(\vartheta_{i,q}) - \varrho_{i,q}(\vartheta_{i,q}(t))| \leqslant u_{i,qN}(1-\tanh(1)) = D_{i,q1}.$$

Accordingly, with the framework of backstepping method, the adaptive neural inner-loop control scheme will be proposed.

The tracking errors are presented as

$$z_{i,q1} = \sum_{m=1}^{M} a_{i,m}(y_{i,q} - y_{m,q}) + b_i(y_{i,q} - y_{q0}), \quad z_{i,q2} = x_{i,q2} - \alpha_{i,q1} - \hbar_{i,q}, \tag{7}$$

where the gains $b_i > 0$ only for the case that the ith follower could receive the information from the leader. The virtual control signal $\alpha_{i,q1}$ and the auxiliary control signal $\hbar_{i,q}$ will be defined later.

Step $i, 1$**.** Design the Lyapunov function candidate as

$$V_{i,q1} = \frac{z_{i,q1}^2}{2} + \frac{\tilde{\Theta}_{i,q1}^2}{2r_{i,q1}},$$

where $r_{i,qj}$ is a positive constant. $\tilde{\Theta}_{i,qj} = \Theta_{i,qj}^* - \hat{\Theta}_{i,qj}$, $\Theta_{i,qj}^* = \max\{\|\theta_{i,qj}^{*\mathrm{T}}\|, \epsilon_{i,qj}^*\}$ $(j = 1, 2)$ with $\epsilon_{i,qj}^*$ being an unknown positive constant. $\hat{\Theta}_{i,qj}$ is the estimate of $\Theta_{i,qj}^*$.

The time derivative of $z_{i,q1}$ is shown as

$$\dot{z}_{i,q1} = (\bar{d}_i + b_i)(z_{i,q2} + f_{i,q1}(\bar{x}_{i,q2}) + \alpha_{i,q1} + \hbar_{i,q}) - \sum_{m=1}^{M} a_{i,m}(x_{m,q2} + f_{m,q1}(\bar{x}_{m,q2})) - b_i\dot{y}_{q0}. \tag{8}$$

Let $F_{i,q1} = (\bar{d}_i + b_i)f_{i,q1}(\bar{x}_{i,q2}) - \sum_{m=1}^{M} a_{i,m}(x_{m,q2} + f_{m,q1}(\bar{x}_{m,q2})) - b_i\dot{y}_{q0}$. The approximation property of radial basis function (RBF) NNs in [40–42] is applied to approximate $F_{i,q1}$, and then, we have

$$\begin{aligned} z_{i,q1}F_{i,q1} =& z_{i,q1}(\theta_{i,q1}^{*\mathrm{T}}\varphi_{i,q1}(Z_{i,q1}) + \epsilon_{i,q1}) \\ \leqslant& |z_{i,q1}|(\|\theta_{i,q1}^{*\mathrm{T}}\|\|\varphi_{i,q1}(Z_{i,q1})\| + \epsilon_{i,q1}^*) \\ \leqslant& |z_{i,q1}|\Theta_{i,q1}^*\Psi_{i,q1}, \end{aligned}$$

where $\Psi_{i,q1} = \|\varphi_{i,q1}(Z_{i,q1,1})\| + 1$, $Z_{i,q1} = [\bar{x}_{i,q2}^{\mathrm{T}}, \bar{x}_{m,q2}^{\mathrm{T}}, y_0, \dot{y}_{q0}]^{\mathrm{T}}$, $Z_{i,q1,1} = [x_{i,q1}^{\mathrm{T}}, x_{m,q1}^{\mathrm{T}}, y_{q0}]^{\mathrm{T}}$. Then, according to $0 \leqslant |\varrho| - \varrho\tanh\left(\frac{\varrho}{\varpi}\right) \leqslant \digamma\varpi, \digamma = 0.2785, \varpi > 0, \varrho > 0$, we have

$$|z_{i,q1}|\Theta_{i,q1}^*\Psi_{i,q1} \leqslant z_{i,q1}\Theta_{i,q1}^*\Psi_{i,q1}\tanh\left(\frac{z_{i,q1}\Psi_{i,q1}}{\varpi_{i,q1}}\right) + \digamma\Theta_{i,q1}^*\varpi_{i,q1}. \tag{9}$$

Construct the virtual controller and adaptive law as

$$\alpha_{i,q1} = -\frac{1}{\bar{d}_i + b_i}\left(c_{i,q1}z_{i,q1} + \hat{\Theta}_{i,q1}\Psi_{i,q1}\tanh\left(\frac{z_{i,q1}\Psi_{i,q1}}{\varpi_{i,q1}}\right)\right) - \hbar_{i,q}, \tag{10}$$

$$\dot{\hat{\Theta}}_{i,q1} = r_{i,q1}z_{i,q1}\Psi_{i,q1}\tanh\left(\frac{z_{i,q1}\Psi_{i,q1}}{\varpi_{i,q1}}\right) - \sigma_{i,q1}\hat{\Theta}_{i,q1}, \tag{11}$$

where $c_{i,q1}$, $\sigma_{i,q1}$, and $\varpi_{i,q1}$ are positive constants.

Substituting (9)–(11) into (8) yields

$$\dot{V}_{i,q1} \leqslant (\bar{d}_i + b_i) z_{i,q1} z_{i,q2} - c_{i,q1} z_{i,q1}^2 + \frac{\sigma_{i,q1} \tilde{\Theta}_{i,q1} \hat{\Theta}_{i,q1}}{r_{i,q1}} + F \Theta_{i,q1}^* \varpi_{i,q1}.$$

To avoid the tedious analytic computation of the virtual control signal $\dot{\alpha}_{i,q1}$, the following first-order SMD is adopted to estimate $\dot{\alpha}_{i,q1}$:

$$\begin{aligned} &\dot{\zeta}_{i,q20} = \eta_{i,q20} = \zeta_{i,q21} - \varepsilon_{i,q20} \left| \zeta_{i,q20} - \alpha_{i,q1} \right|^{1/2} \operatorname{sign}\left(\zeta_{i,q20} - \alpha_{i,1} \right), \\ &\dot{\zeta}_{i,q21} = -\varepsilon_{i,q21} \operatorname{sign}\left(\zeta_{i,q21} - \eta_{i,q20} \right), \quad \dot{\alpha}_{i,q1} = \eta_{i,q20} + \varsigma_{i,q1}, \quad |\varsigma_{i,q1}| < \varsigma_{i,q1}^*, \end{aligned} \tag{12}$$

where $\varsigma_{i,q1}$ stands for an estimate error, $\varsigma_{i,q1}^*$ denotes an unknown positive constant.

To reduce the updating numbers and alleviate the communication burden, an adaptive event triggering mechanism is constructed for the nonstrict-feedback attitude system of UAV.

The control signal of event triggering is presented as

$$\vartheta_{i,q}(t) = \omega_{i,q}(t_{i,q}^h), \ \forall t \in [t_{i,q}^h, t_{i,q}^{h+1}), \quad t_{i,q}^{h+1} = \inf\{ t > t_{i,q}^h \mid |\varepsilon_{i,q}(t)| - \lambda_{i,q} |\vartheta_{i,q}(t)| - \mu_{i,q} \geqslant 0 \}, \tag{13}$$

where $\omega_{i,q}(t)$ stands for the intermediate continuous control signal. $\lambda_{i,q} \in (0,1)$ and $\mu_{i,q} > 0$ are the design parameters. $\varepsilon_{i,q}(t) = \omega_{i,q}(t) - \vartheta_{i,q}(t)$ is the measured error. $t_{i,q}^h$, $h \in \mathbb{Z}^+$ is called as input updating times. When $t \in [t_{i,q}^h, t_{i,q}^{h+1})$, the control signal $\vartheta_{i,q}(t)$ is a constant.

When $t \in [t_{i,q}^h, t_{i,q}^{h+1})$, one has

$$|\omega_{i,q}(t) - \vartheta_{i,q}(t)| \leqslant \lambda_{i,q} |\vartheta_{i,q}(t)| + \mu_{i,q}.$$

From (13), it shows that

$$\vartheta_{i,q}(t) = \frac{\omega_{i,q}(t)}{1 + k_{i,q}^1(t) \lambda_{i,q}} - \frac{k_{i,q}^2(t) \mu_{i,q}}{1 + k_{i,q}^1(t) \lambda_{i,q}}, \tag{14}$$

where $|k_{i,q}^1(t)| \leqslant 1$ and $|k_{i,q}^2(t)| \leqslant 1$.

Design the intermediate continuous control signal as

$$\omega_{i,q}(t) = -(1 + \lambda_{i,q}) \left(\alpha_{i,q2} \tanh\left(\frac{z_{i,q2} \alpha_{i,q2}}{\varpi_{i,q2}} \right) + \bar{\mu}_{i,q} \tanh\left(\frac{z_{i,q2} \bar{\mu}_{i,q}}{\varpi_{i,q2}} \right) \right), \tag{15}$$

where $\bar{\mu}_{i,q} > \frac{\mu_{i,q}}{1 - \lambda_{i,q}}$ is a positive constant to be determined. $\varpi_{i,q2}$ is a positive constant to be given.

Subsequently, the stability of closed-loop system will be proved by the proposed adaptive event triggering control scheme.

Step $i, 2$**.** To deal with the issue of input saturation, we introduce a dynamic system subject to auxiliary design function $\hbar_{i,q}$ as follows:

$$\dot{\hbar}_{i,q} = -\hbar_{i,q} + \varrho_{i,q}(\vartheta_{i,q}) - \vartheta_{i,q}.$$

The Lyapunov function candidate is defined as

$$V_{i,q2} = V_{i,q1} + \frac{z_{i,q2}^2}{2} + \frac{\tilde{d}_{i,q}^2}{2\bar{r}_{i,q}} + \frac{\tilde{\Theta}_{i,q2}^2}{2 r_{i,q2}},$$

where $\bar{r}_{i,q}$ is a positive constant, $\hat{d}_{i,q}$ is the estimation of $d_{i,q}^*$ and $\tilde{d}_{i,q} = d_{i,q}^* - \hat{d}_{i,q}$.

Similarly, differentiating $V_{i,q2}$ yields

$$\begin{aligned} \dot{V}_{i,q2} =& \dot{V}_{i,q1} + z_{i,q2}(\vartheta_{i,q} + \varsigma_{i,q}(\vartheta_{i,q}(t)) + \hbar_{i,q} + f_{i,q2}(\bar{x}_{i,q2}) + d_{i,q} - (\eta_{i,q20} + \varsigma_{i,q1})) - \frac{\tilde{d}_{i,q} \dot{\hat{d}}_{i,q}}{\bar{r}_{i,q}} - \frac{\tilde{\Theta}_{i,q2} \dot{\hat{\Theta}}_{i,q2}}{r_{i,q2}}. \end{aligned} \tag{16}$$

According to $0 \leqslant |\varrho| - \varrho \tanh\left(\frac{\varrho}{\varpi}\right) \leqslant \digamma\varpi, \digamma = 0.2785, \varpi > 0, \varrho > 0$, $-\varrho \tanh\left(\frac{\varrho}{\varpi}\right) \leqslant 0$, $|k_{i,q}^1(t)| \leqslant 1$, $|k_{i,q}^2(t)| \leqslant 1$, and $z_{i,q}\omega_{i,q}(t) \leqslant 0$, the following inequalities hold:

$$\begin{aligned} z_{i,q2}\vartheta_{i,q} &\leqslant \frac{z_{i,q2}\omega_{i,q}(t)}{1+k_{i,q}^1(t)\lambda_{i,q}} - \frac{z_{i,q2}k_{i,q}^2(t)\mu_{i,q}}{1+k_{i,q}^1(t)\lambda_{i,q}} \\ &\leqslant \frac{z_{i,q2}\omega_{i,q}(t)}{1+\lambda_{i,q}} + |z_{i,q2}\bar{\mu}_{i,q}| \\ &\leqslant -z_{i,q2}\alpha_{i,q2}\tanh\left(\frac{z_{i,q2}\alpha_{i,q2}}{\varpi_{i,q2}}\right) + \digamma\varpi_{i,q2} \\ &\leqslant 2\digamma\varpi_{i,q2} - z_{i,q2}\alpha_{i,q2}. \end{aligned} \tag{17}$$

According to Lemmas 1 and 2 and Young's inequality, one gets

$$\begin{aligned} &z_{i,q2}(\varsigma_{i,q}(\vartheta_{i,q}) - \varsigma_{i,q1}) \leqslant z_{i,q2}^2 + \frac{\varsigma_{i,q1}^{*2}}{2} + \frac{D_{i,q1}^2}{2}, \\ &z_{i,q2}d_{i,q} \leqslant |z_{i,q2}|d_{i,q}^* + (\hat{d}_{i,q} + \tilde{d}_{i,q} - d_{i,q}^*)z_{i,q2}\tanh\left(\frac{z_{i,q2}}{\varpi_{i,q2}}\right), \\ &z_{i,q2}f_{i,q2}(\bar{x}_{i,q2}) = z_{i,q2}(\theta_{i,q2}^{*\mathrm{T}}\varphi_{i,q2}(\bar{x}_{i,q2}) + \epsilon_{i,q2}) \leqslant |z_{i,q2}|\Theta_{i,q2}^*\Psi_{i,q2}, \end{aligned} \tag{18}$$

where $\Psi_{i,q2} = \|\varphi_{i,q2}(\bar{x}_{i,q2})\| + 1$.

The virtual controller and adaptive laws are set as

$$\begin{aligned} &\alpha_{i,q2} = c_{i,q2}z_{i,q2} + z_{i,q2} + (b_i + \bar{d}_i)z_{i,q1} + \hbar_{i,q} - \eta_{i,q20} + \hat{\Theta}_{i,q}\Psi_{i,q2}\tanh\left(\frac{z_{i,q2}\Psi_{i,q2}}{\varpi_{i,q2}}\right) + \hat{d}_{i,q}\tanh\left(\frac{z_{i,q2}}{\varpi_{i,q2}}\right), \\ &\dot{\hat{d}}_{i,q} = \bar{r}_{i,q}z_{i,q2}\tanh\left(\frac{z_{i,q2}}{\varpi_{i,q2}}\right) - \bar{\sigma}_{i,q}\hat{d}_{i,q}, \quad \dot{\hat{\Theta}}_{i,q2} = r_{i,q2}z_{i,q2}\Psi_{i,q2}\tanh\left(\frac{z_{i,q2}\Psi_{i,q2}}{\varpi_{i,q2}}\right) - \sigma_{i,q2}\hat{\Theta}_{i,q2}, \end{aligned} \tag{19}$$

where $c_{i,q2}$, $\bar{\sigma}_{i,q}$, and $\sigma_{i,q2}$ are given constants.

Similar to the analysis in Step $i,1$, $\dot{V}_{i,q2}$ is transformed as

$$\dot{V}_{i,q2} \leqslant -\sum_{j=1}^{2} c_{i,qj}z_{i,qj}^2 - \sum_{j=1}^{2}\frac{\sigma_{i,qj}\tilde{\Theta}_{i,qj}^2}{2r_{i,qj}} - \frac{\bar{\sigma}_i\tilde{d}_{i,q}^2}{2\bar{r}_{i,q}} + \Lambda_{i,q}, \tag{20}$$

where $\Lambda_{i,q} = \sum_{j=1}^{2}\frac{\sigma_{i,qj}\Theta_{i,qj}^{*2}}{2r_{i,qj}} + \frac{\bar{\sigma}_{i,q}d_{i,q}^{*2}}{2\bar{r}_{i,q}} + \sum_{j=1}^{2}\digamma\Theta_{i,qj}^*\varpi_{i,qj} + 2\digamma\varpi_{i,q2} + d_{i,q}^*\digamma\varpi_{i,q2} + \frac{\varsigma_{i,q1}^{*2}}{2} + \frac{D_{i,q1}^2}{2}$.

Then, one obtains

$$\dot{V}_{i,q2} \leqslant -\mathcal{L}_{i,q}V_{i,q2} + \Lambda_{i,q}, \tag{21}$$

where $\mathcal{L}_{i,q} = \min\{2c_{i,qj}, \sigma_{i,qj}, \bar{\sigma}_{i,q}, i = 1,\ldots,M, j = 1,2, q = 1,2,3\}$ and $c_{i,q1} > 0$, $\sigma_{i,qj} > 0$, $\bar{\sigma}_{i,q} > 0$.

According to the previous development, the main results are summarised as the following theorem.

Theorem 1. Under Assumptions 1 and 2, the first-order SMD (12), the event-triggered mechanism (13), the intermediate control signal (15), and the adaptive laws (11) and (19) guarantee that all signals of the closed-loop attitude system (6) are SGUUB. Moreover, the Zeno behavior can be avoided.

Proof. The Lyapunov function candidate of the whole attitude systems is $V = \sum_{i=1}^{M}\sum_{q=1}^{3}V_{i,q2}$. From (21), we have

$$\dot{V} \leqslant -\mathcal{L}_sV + \Lambda_s, \tag{22}$$

where $\mathcal{L}_s = \min\{\mathcal{L}_1, \mathcal{L}_2, \ldots, \mathcal{L}_M\}$, $\mathcal{L}_i = \min\{\mathcal{L}_{i,1}, \mathcal{L}_{i,2}, \mathcal{L}_{i,3}\}$, and $\Lambda_s = \sum_{i=1}^{M}\sum_{q=1}^{3}\Lambda_{i,q}$. Subsequently, integrating (22) over $[0,t]$, one has

$$0 \leqslant V(t) \leqslant \left(V(0) - \frac{\Lambda_s}{\mathcal{L}_s}\right)\mathrm{e}^{-\mathcal{L}_st} + \frac{\Lambda_s}{\mathcal{L}_s}. \tag{23}$$

Then, considering the definitions of $V_{i,q1}$ and $V_{i,q2}$, the following inequality holds: $|z_{i,q1}|^2 \leqslant 2\mathrm{e}^{-\mathcal{L}_s t}V(0)+\frac{2\Lambda_s}{\mathcal{L}_s}(1-\mathrm{e}^{-\mathcal{L}_s t})$. Then, we have $|z_{i,q1}| \leqslant \sqrt{\frac{2\Lambda_s}{\mathcal{L}_s}}$ as $t \to \infty$. Therefore, it can be seen that the tracking error $z_{i,q1}$ can be controlled arbitrarily small via choosing the appropriate parameters. According to (23), all signals in the closed-loop system are SGUUB.

Then, we need to prove that the proposed adaptive NN event-triggered control scheme can avoid Zeno behavior. In this case, a time constant $t^*_{i,q} > 0$ can be found to satisfy $\forall h \in \mathbb{Z}^+, \{t^{h+1}_{i,q} - t^h_{i,q} \geqslant t^*_{i,q}\}$.

With $\epsilon_{i,q}(t) = \omega_{i,q}(t) - u_{i,q}(t), \forall t_q \in [t^*_{i,q}, t^{h+1}_{i,q})$, we obtain $\frac{\mathrm{d}}{\mathrm{d}t}|\epsilon_{i,q}| = \frac{\mathrm{d}}{\mathrm{d}t}(\epsilon_{i,q} \times \epsilon_{i,q})^{\frac{1}{2}} = \mathrm{sign}(\epsilon_{i,q})\dot{\epsilon}_{i,q} \leqslant |\dot{\omega}_{i,q}|$. From (19), we find that $\omega_{i,q}$ is differentiable and $\dot{\omega}_{i,q}$ is a function subject to the bounded signals in the closed-loop system. Consequently, there exists a constant $\iota_{i,q} > 0$ to satisfy $|\dot{\omega}_{i,q}| \leqslant \iota_{i,q}$. For $\epsilon_{i,q}(t^h_{i,q}) = 0$ and $\lim_{t_q \to t^{h+1}_{i,q}} \epsilon_{i,q}(t) = \mu_{i,q}$, the lower bound of inter-execution intervals $t^*_{i,q} \geqslant \frac{\mu_{i,q}}{\iota_{i,q}}$ can be found to exclude Zeno behavior.

3.2 Design of adaptive outer-loop controller

According to (3), the position equation of UAV i can be constructed as

$$\dot{\eta}_{n,1} = \eta_{n,2} + g_{n,1}, \quad \dot{\eta}_{n,2} = \ell u_n + g_{n,2} + d_n, \quad y_n = \eta_{n,1}, \quad n = 1, 2, 3, \tag{24}$$

where $\eta_{1,1} = x$, $\eta_{1,2} = v_x$, $\eta_{2,1} = y$, $\eta_{2,2} = v_y$, $\eta_{3,1} = z$, $\eta_{3,2} = v_z$, $g_{n,1}$ and $g_{n,2}$ stand for the neglected and unmodeled parts of the position system, respectively. The system output y_n satisfies Assumption 3. $\ell = \frac{1}{m}$. u_1, u_2, and u_3 can be expressed by $u_1 = (C_{\psi_i}S_{\theta_i}C_{\phi_i} + S_{\psi_i}S_{\phi_i})U_1, u_2 = (S_{\psi_i}S_{\theta_i}C_{\phi_i} - C_{\psi_i}S_{\phi_i})U_1$, and $u_3 = (C_{\theta_i}C_{\phi_i})U_1 - mg$. $d_1 = \frac{k_1}{m}\dot{x}$, $d_2 = \frac{k_2}{m}\dot{y}$, $d_3 = \frac{k_3}{m}\dot{z}$.

According to the definitions of u_1, u_2, u_3, we have

$$\begin{aligned} &U_1 = \sqrt{u_1^2 + u_2^2 + (u_3 + mg)^2}, \quad \phi_d = \arcsin\left(\frac{u_1\sin(\psi_d) - u_2\cos(\psi_d)}{U_1}\right), \\ &\theta_d = \arctan\left(\frac{u_1\cos(\psi_d) + u_2\sin(\psi_d)}{u_3 + mg}\right). \end{aligned} \tag{25}$$

Remark 3 ([4,33]). u_1, u_2, u_3 can be designed later. ψ_d, θ_d, ϕ_d are the reference trajectories of ψ_i, θ_i, ϕ_i. ψ_d is regarded as an extra reference signal to be given. The parameters θ_d and ϕ_d can be calculated by (25). According to Theorem 1, ψ_i, θ_i, ϕ_i can rapidly converge to ψ_d, θ_d, ϕ_d.

The changes of coordinates are presented as

$$s_{n,1} = \eta_{n,1} - y_{n,d}, \quad s_{n,2} = \eta_{n,2} - a_{n,1}, \tag{26}$$

where $a_{n,1}$ is the virtual control signal to be designed later. $y_{n,d}$ is the desired trajectory of y_n.

Step $n, 1$**.** Time-varying bounds $k_{an,1}(t)$ and $k_{bn,1}(t)$ of $s_{n,1}$ are given as

$$k_{an,1}(t) = y_{n,d}(t) - \underline{k}_{cn,1}(t), \quad k_{bn,1}(t) = \overline{k}_{cn,1}(t) - y_{n,d}(t). \tag{27}$$

The Lyapunov function candidate $V_{n,1}$ is considered as

$$V_{n,1} = \frac{q_n(s_{n,1})}{2}\ln\frac{k^2_{bn,1}}{k^2_{bn,1} - s^2_{n,1}} + \frac{1 - q_n(s_{n,1})}{2}\ln\frac{k^2_{an,1}}{k^2_{an,1} - s^2_{n,1}} + \frac{\tilde{\Theta}^2_{n,1}}{2r_{n,1}}, \tag{28}$$

where $q_n(s_{n,1}) = 0$ for $s_{n,1} \leqslant 0$, and $q_n(s_{n,1}) = 1$ for $s_{n,1} > 0$.

Let $\chi_{an,1} = \frac{s_{n,1}}{k_{an,1}}, \chi_{bn,1} = \frac{s_{n,1}}{k_{bn,1}}, \chi_n = q_n(s_{n,1})\chi_{bn,1} + (1 - q_n(s_{n,1}))\chi_{an,1}$ denote the coordinate conversions of the error. To facilitate the design of adaptive backstepping control, Eq. (28) can be transformed into

$$V_{n,1} = \frac{1}{2}\ln\frac{1}{1 - \chi_n^2} + \frac{\tilde{\Theta}^2_{n,1}}{2r_{n,1}},$$

where $r_{n,j}, j = 1, 2$ are positive constants. $\Theta^*_{n,j} = \max\{\|\theta^{*\mathrm{T}}_{n,j}\|, \epsilon^*_{n,j}\}$ with $\epsilon^*_{n,j}$ being an unknown positive constant. $\hat{\Theta}_{n,j}$ is the estimate of $\Theta^*_{n,j}$ and $\hat{\Theta}_{n,j} = \Theta^*_{n,j} - \tilde{\Theta}_{n,j}$.

Via $s_{n,1}=y_n-y_{n,d}$ and $s_{n,2}=\eta_{n,2}-a_{n,1}$, the time derivative of $V_{n,1}$ can be calculated as

$$\begin{aligned}\dot{V}_{n,1}=&\frac{q_n\chi_{bn}}{k_{bn,1}(1-\chi_{bn}^2)}\left(s_{n,2}+a_{n,1}+g_{n,1}-s_{n,1}\frac{\dot{k}_{bn,1}}{k_{bn,1}}-\dot{y}_{n,d}\right)-\frac{\tilde{\Theta}_{n,1}\dot{\hat{\Theta}}_{n,1}}{r_{n,1}}\\&+\frac{(1-q_n)\chi_{an}}{k_{an,1}(1-\chi_{an}^2)}\left(s_{n,2}+a_{n,1}+g_{n,1}-\dot{y}_{n,d}-s_{n,1}\frac{\dot{k}_{an,1}}{k_{an,1}}\right).\end{aligned}\tag{29}$$

Note that $\frac{q_n\chi_{bn}}{k_{bn,1}(1-\chi_{bn}^2)}+\frac{(1-q_n)\chi_{an}}{k_{an,1}(1-\chi_{an}^2)}=\frac{q_ns_{n,1}}{k_{bn,1}^2-s_{n,1}^2}+\frac{(1-q_n)s_{n,1}}{k_{an,1}^2-s_{n,1}^2}=\xi_ns_{n,1},\xi_n=\frac{q_n}{k_{bn,1}^2-s_{n,1}^2}+\frac{(1-q_n)}{k_{an,1}^2-s_{n,1}^2}$. With Lemma 1, Young's inequality and $0\leqslant|\varrho|-\varrho\tanh\left(\frac{\varrho}{\varpi}\right)\leqslant\digamma\varpi,\varpi>0,\varrho\in\mathbb{R}$, one has

$$\begin{aligned}\xi_ns_{n,1}g_{n,1}&=\xi_ns_{n,1}(\theta_{n,1}^{*\mathrm{T}}\varphi_{n,1}(Z_{n,1})+\epsilon_{n,1})\\&\leqslant\xi_ns_{n,1}\Theta_{n,1}^*\Psi_{n,1}\tanh\left(\frac{\xi_ns_{n,1}\Psi_{n,1}}{\varpi_{n,1}}\right)+\digamma\Theta_{n,1}^*\varpi_{n,1},\end{aligned}\tag{30}$$

where $Z_{n,1}=[x_{n,1},x_{n,2}]^{\mathrm{T}}$, $\Psi_{n,1}=\|\varphi_{n,1}(Z_{n,1,1})\|+1$, $Z_{n,1,1}=[x_{n,1}]^{\mathrm{T}}$.

The virtual controller and adaptive law are given as

$$a_{n,1}=-\left((c_{n,1}+\bar{c}_{n,1}(t))s_{n,1}-\dot{y}_{n,d}+\hat{\Theta}_{n,1}\Psi_{n,1}\tanh\left(\frac{\xi_ns_{n,1}\Psi_{n,1}}{\varpi_{n,1}}\right)\right),\tag{31}$$

$$\dot{\hat{\Theta}}_{n,1}=r_{n,1}\xi_ns_{n,1}\Psi_{n,1}\tanh\left(\frac{\xi_ns_{n,1}\Psi_{n,1}}{\varpi_{n,1}}\right)-\sigma_{n,1}\hat{\Theta}_{n,1},\tag{32}$$

where $c_{n,1}>0$, $r_{n,1}>0$, $\varpi_{n,1}>0$, and $\sigma_{n,1}>0$, $\bar{c}_{n,1}(t)=\sqrt{(\frac{\dot{k}_{bn,1}}{k_{bn,1}})^2+(\frac{\dot{k}_{an,1}}{k_{an,1}})^2+\Phi}$ and $\bar{c}_{n,1}(t)+(1-q_n)\frac{\dot{k}_{an,1}}{k_{an,1}}+q_n\frac{\dot{k}_{bn,1}}{k_{bn,1}}\geqslant0$.

Substituting (30)–(32) into (29), one has

$$\dot{V}_{n,1}\leqslant-c_{n,1}\frac{\chi_n^2}{1-\chi_n^2}+\digamma\Theta_{n,1}^*\varpi_{n,1}+\frac{\sigma_{n,1}\tilde{\Theta}_{n,1}\hat{\Theta}_{n,1}}{r_{n,1}}+\xi_ns_{n,1}s_{n,2}.\tag{33}$$

Remark 4. In this paper, the proposed time-varying BLF-based control strategy can be extended to handle the static output constraints and time-varying full state constraints.

Similarly as (12), to reduce the computational complexity with $\dot{\alpha}_{n,1}$, the first-order SMD consisting of $\zeta_{n,20},\zeta_{n,21},\eta_{n,20},\varepsilon_{n,20},\varepsilon_{n,21}$, and $\varsigma_{n,1}$ is used to address the virtual control signal $\dot{a}_{n,1}$:

$$\dot{a}_{n,1}=\eta_{n,20}+\varsigma_{n,1},\quad|\varsigma_{n,1}|<\varsigma_{n,1}^*,\tag{34}$$

where $\varsigma_{n,1}^*$ is an unknown positive constant.

Step $n,2$**.** The Lyapunov function candidate is defined as

$$V_{n,2}=V_{n,1}+\frac{s_{n,2}^2}{2}+\frac{\tilde{\Theta}_{n,2}^2}{2r_{n,2}}+\frac{\tilde{d}_n^2}{2\bar{r}_n},$$

where $\bar{r}_n$ is a positive constant. $\tilde{d}_n=d_n^*-\hat{d}_n$, $\hat{d}_n$ stands for the estimation of d_n^*.

The controller u_n, adaptive laws $\dot{\hat{d}}_n$ and $\dot{\hat{\Theta}}_{n,2}$ are given as

$$u_n=-\frac{1}{\ell}\left(c_{n,2}s_{n,2}+\frac{s_{n,2}}{2}-\eta_{n,20}+\hat{d}_n\tanh\left(\frac{s_{n,2}}{\varpi_{n,2}}\right)+\hat{\Theta}_{n,2}\Psi_{n,2}\tanh\left(\frac{s_{n,2}\Psi_{n,2}}{\varpi_{n,2}}\right)+\xi_ns_{n,1}\right),\tag{35}$$

$$\dot{\hat{d}}_n=\bar{r}_ns_{n,2}\tanh\left(\frac{s_{n,2}}{\varpi_{n,2}}\right)-\bar{\sigma}_n\hat{d}_n,\quad\dot{\hat{\Theta}}_{n,2}=r_{n,2}s_{n,2}\Psi_{n,2}\tanh\left(\frac{s_{n,2}\Psi_{n,2}}{\varpi_{n,2}}\right)-\sigma_{n,2}\hat{\Theta}_{n,2},\tag{36}$$

where $c_{n,2}$, $\bar{\sigma}_n$, $\varpi_{n,2}$, and $\sigma_{n,2}$ are given constants.

Let $\Psi_{n,2} = \|\varphi_{n,2}(Z_{n,2,1})\| + 1$ and $Z_{n,2,1} = [x_{n,1}, x_{n,2}]^{\mathrm{T}}$. Via the same calculation procedure as in (18), $\dot{V}_{n,2}$ can be arranged as

$$\dot{V}_{n,2} \leqslant -\frac{c_{n,1}\chi_n^2}{1-\chi_n^2} - c_{n,2}s_{n,2}^2 - \sum_{j=1}^{2}\frac{\sigma_{n,j}\tilde{\Theta}_{n,j}^2}{2r_{n,j}} - \frac{\bar{\sigma}_n\tilde{d}_n^2}{2\bar{r}_n} + \Lambda_{n,p}$$

with $\Lambda_{n,p} = \sum_{j=1}^{2}\frac{\sigma_{n,j}\Theta_{n,j}^{*2}}{2r_{n,j}} + \frac{\bar{\sigma}_n d_n^{*2}}{2\bar{r}_n} + \sum_{j=1}^{2}F\Theta_{n,j}^{*}\varpi_{n,j} + d_n^{*}F\varpi_{n,2} + \frac{\varsigma_{n,1}^{*2}}{2}$.

Furthermore, letting $\mathcal{L}_{n,p} = \min\{2c_{n,1}, 2c_{n,2}, \sigma_{n,j}, \bar{\sigma}_n\}$, we have

$$\dot{V}_{n,2} \leqslant -\mathcal{L}_{n,p}V_{n,2} + \Lambda_{n,p}. \tag{37}$$

Theorem 2. For the position system (24) with a nonstrict-feedback structure, under Assumptions 1–3, Lemmas 1–4, the controllers (31) and (35), the adaptive laws (32) and (36), and SMD (34), all signals involved in the closed-loop system can be ensured to be SGUUB.

Proof. The Lyapunov candidate function of the position system is $V_p = \sum_{n=1}^{3}V_{n,2}$. From (37), we have

$$\dot{V}_p \leqslant -\mathcal{L}_pV_p + \Lambda_p, \tag{38}$$

where $\mathcal{L}_p = \min\{\mathcal{L}_{1,p}, \mathcal{L}_{2,p}, \mathcal{L}_{3,p}\}$. $\Lambda_p = \sum_{n=1}^{3}\Lambda_{n,p}$.

Integrating both sides of (38) with $t > 0$ yields

$$0 \leqslant V_p(t) \leqslant \left(V_p(0) - \frac{\Lambda_p}{\mathcal{L}_p}\right)\mathrm{e}^{-\mathcal{L}_pt} + \frac{\Lambda_p}{\mathcal{L}_p}, \tag{39}$$

where if $V_p(0) \leqslant V_p^*$ with V_p^* being a constant, then $V_p(t) \leqslant V_p^* + \frac{\Lambda_p}{\mathcal{L}_p}, \forall t > 0$.

From (28) and (39), we can obtain that

$$\frac{q_n(s_{n,1})}{2}\ln\frac{k_{bn,1}^2}{k_{bn,1}^2(t)-s_{n,1}^2} + \frac{1-q_n(s_{n,1})}{2}\ln\frac{k_{an,1}^2}{k_{an,1}^2-s_{n,1}^2} \leqslant \left(V_p(0) - \frac{\Lambda_p}{\mathcal{L}_p}\right)\mathrm{e}^{-\mathcal{L}_pt} + \frac{\Lambda_p}{\mathcal{L}_p}. \tag{40}$$

With the help of $k_{an,1}(t) < s_{n,1}(t) < k_{bn,1}(t)$, we have $k_{bn,1}^2(t) - s_{n,1}^2 > 0$ and $k_{an,1}^2 - s_{n,1}^2 < 0$. When $q_n(s_{n,1}) = 0$ and $s_{n,1} > 0$, Eq. (40) can be represented as

$$q_n(s_{n,1})\frac{k_{bn,1}^2}{k_{bn,1}^2(t) - s_{n,1}^2} \leqslant \mathrm{e}^{2((V_p(0)-\frac{\Lambda_p}{\mathcal{L}_p})\mathrm{e}^{-\mathcal{L}_pt}+\frac{\Lambda_p}{\mathcal{L}_p})}. \tag{41}$$

Then, it follows that

$$|s_{n,1}| \leqslant k_{bn,1}(t)\sqrt{1 - \mathrm{e}^{-2((V_p(0)-\frac{\Lambda_p}{\mathcal{L}_p})\mathrm{e}^{-\mathcal{L}_pt}+\frac{\Lambda_p}{\mathcal{L}_p})}}. \tag{42}$$

Then, we get $|s_{n,1}| \leqslant k_{bn,1}(t)\sqrt{1-\mathrm{e}^{-2\frac{\Lambda_p}{\mathcal{L}_p}}}$ as $t \to \infty$. Similarly, $s_{n,1} \geqslant -k_{an,1}(t)\sqrt{1-\mathrm{e}^{-2\frac{\Lambda_p}{\mathcal{L}_p}}}$ when $q(s_1) = 1$ and $s_{n,1} \leqslant 0$. Therefore, it follows from $-k_{an,1}(t)\sqrt{1-\mathrm{e}^{-2\frac{\Lambda_p}{\mathcal{L}_p}}} \leqslant s_{n,1} \leqslant k_{bn,1}(t)\sqrt{1-\mathrm{e}^{-2\frac{\Lambda_p}{\mathcal{L}_p}}}$ that the tracking error $s_{n,1}$ can be controlled arbitrarily small via choosing the appropriate parameters. According to (39), all signals in the closed-loop system are SGUUB.

4 Simulation results

For multi-UAV systems, some simulation results are presented to demonstrate the effectiveness and validity of the proposed double-loop control strategy and event triggering mechanism under the communication graph as shown in Figure 3.

To track the vertical helix flight trajectory, the desired signals of the task are set as $y_{1,d} = 0.5\sin(t)$, $y_{2,d} = 0.5\cos(t)$, $y_{3,d} = 0.5t$, $y_{q0} = [\phi_d, \theta_d, \varphi_d]^{\mathrm{T}}$, $\varphi_d = \sin(0.5t)$, $k_{a1,1} = 0.1\sin(t) + 0.5$, $k_{b1,1} = 0.1\cos(t) + 0.6 - 0.5\sin(t)$, $k_{a2,1} = 0.1\cos(t) + 0.5$, $k_{b2,1} = 0.1\sin(t) + 0.6 - 0.5\cos(t)$, $k_{a3,1} = -0.8$, $k_{b3,1} = 0.8$. Moreover, simulation parameters of the task are given as follows: $g_{n,1} = 0.1\sin(x_{n,1}x_{n,2})$, $g_{n,2} =$

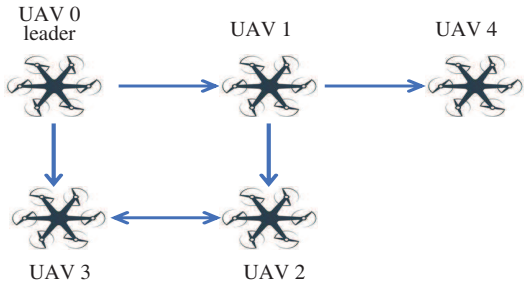

Figure 3 (Color online) Directed communication topology graph.

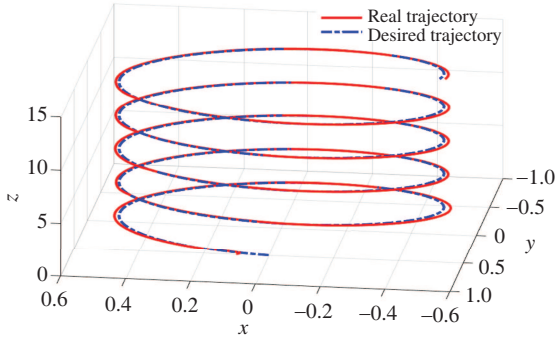

Figure 4 (Color online) 3D tracking trajectories of the vertical helix flight.

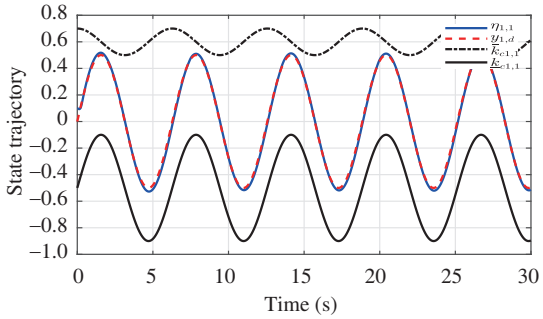

Figure 5 (Color online) The trajectories of state $\eta_{1,1}$ and desired signal $y_{1,d}$.

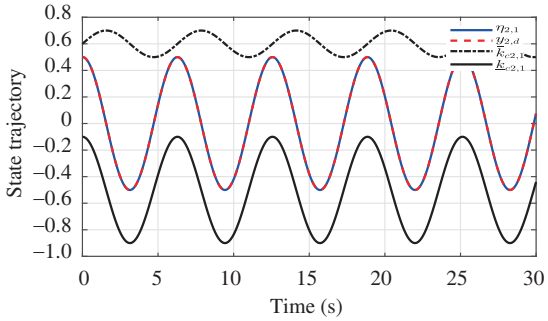

Figure 6 (Color online) The trajectories of state $\eta_{2,1}$ and desired signal $y_{2,d}$.

$(x_{n,1}+x_{n,2})\cos(x_{n,1})$, $f_{i,q1}=0.1\sin(x_{i,q1})\sin(x_{i,q2})$, $x_{1,q1}(0)=[0.1,0.2,0.2]^{\mathrm{T}}$, $x_{2,q1}(0)=[0.2,0.1,0.2]^{\mathrm{T}}$, $x_{3,q1}(0)=[0.3,0.4,0.1]^{\mathrm{T}}$, $x_{4,q1}(0)=[0.5,0.1,0.5]^{\mathrm{T}}$, $u_{i,qN}=40$, $J_x=1.2416$, $J_y=1.2416$, $J_z=2.4832$ $m=2$, $\Phi=0.1$, $\varepsilon_{i,q20}=[0.2,0.2,0.2]^{\mathrm{T}}$, $\varepsilon_{i,q21}=[0.2,0.2,0.2]^{\mathrm{T}}$, $\varepsilon_{n,20}=0.2$, $\varepsilon_{n,21}=0.2$, $\varpi_{i,12}=0.02$, $\varpi_{n,2}=0.02$, $\omega_{i,q1}=0.1$, $\omega_{i,q2}=0.1$, $\mu_{1,q}=0.05$, $\mu_{2,q}=0.1$, $\mu_{3,q}=0.1$, $\mu_{4,q}=0.1$, $\lambda_{1,q}=0.8$, $\lambda_{2,q}=0.7$, $\lambda_{3,q}=0.78$, $\lambda_{4,q}=0.6$, $c_{1,q1}=[2,3,6]^{\mathrm{T}}$, $c_{1,q2}=[2,2.5,2.5]^{\mathrm{T}}$, $c_{2,q1}=[6,8,12]^{\mathrm{T}}$, $c_{2,q2}=[0.4,1,0.4]^{\mathrm{T}}$, $c_{3,q1}=[4,8,8]^{\mathrm{T}}$, $c_{3,q2}=[8,7.4,8]^{\mathrm{T}}$, $c_{4,q1}=[8,5,8]^{\mathrm{T}}$, $c_{4,q2}=[5,5.8,5.8]^{\mathrm{T}}$, $c_{n,1}=[10,18,10]^{\mathrm{T}}$, $c_{n,2}=[10,40,40]^{\mathrm{T}}$, $r_{i,q1}=[0.1,0.1,0.1]^{\mathrm{T}}$, $\sigma_{i,q1}=[100,80,80]^{\mathrm{T}}$, $r_{i,q2}=[0.1,0.1,0.1]$, $\sigma_{i,q2}=[80,80,80]^{\mathrm{T}}$, $\bar{r}_{i,q}=[0.01,0.01,0.01]^{\mathrm{T}}$, $\bar{\sigma}_{i,q}=[20,20,20]^{\mathrm{T}}$, $r_{n,1}=[0.1,0.1,0.1]^{\mathrm{T}}$, $\sigma_{n,1}=[1.5,1.5,1.5]^{\mathrm{T}}$, $r_{n,2}=[0.1,0.1,0.1]^{\mathrm{T}}$, $\sigma_{n,2}=[1.5,1.5,1.5]^{\mathrm{T}}$, $\bar{r}_n=[0.1,0.1,0.1]^{\mathrm{T}}$, $\bar{\sigma}_n=[1.5,1.5,1.5]^{\mathrm{T}}$. The sampling period is 0.001 s.

In the attitude systems, $f_{1,q2}$ and $f_{2,q2}$ are approximated by an RBF NN, which contains 7 nodes with the center evenly spaced in $[-2,2]$ and the Gaussian-type function width being equal to 2. In the position systems, to approximate $g_{n,1}$ and $g_{n,2}$, we choose 7 nodes with the center uniformly distributed in $[-2,2]$. For UAV systems with time-varying output constraints and input saturation, the following simulation results are presented. Figure 4 illustrates the 3D tracking trajectory of the nonlinear position system of UAV 1, the desired trajectory of vertical helix flight can be found in many practical scenarios such as flying in the staircase. More details of the good performance on tracking trajectories are depicted in Figures 5–7, which show the desired signals $y_{1,d}$, $y_{2,d}$, $y_{3,d}$, the tracking trajectories of states $\eta_{1,1}$, $\eta_{2,1}$, $\eta_{3,1}$, and the asymmetric time-varying output constraints $\bar{k}_{c1,1}, \underline{k}_{c1,1}, \bar{k}_{c2,1}, \underline{k}_{c2,1}, \bar{k}_{c3,1}, \underline{k}_{c3,1}$. It can be learnt from Figures 5–7 that the outputs of the position system of UAV 1 not only satisfy the time-varying constraints, but also converge to a small neighborhood of the desired trajectories. Figure 8 depicts the trajectories of tracking errors $s_{n,1}$ under SMD and DSC approaches, which indicates that SMD technique is more effective than DSC method. On the other hand, Figures 9–11 display the trajectories of the desired signals and the outputs of the attitude systems of UAV i ($i=1,2,3,4$). It should be noticed that the desired signals of θ_0 and ϕ_0 are not given directly but are obtained through (25). Moreover, the actual event triggering control signals $u_{i,\phi}(\vartheta_i)$, $u_{i,\theta}(\vartheta_i)$, and $u_{i,\psi}(\vartheta_i)$ with actuator saturation are depicted in Figures 12–14. The release instants of event triggering signal $u_{i,1}(\vartheta_{i,1})$ are presented in Figure 15, where the actuator of UAV i only uses 1688, 1110, 2072, and 1425 samples, respectively,

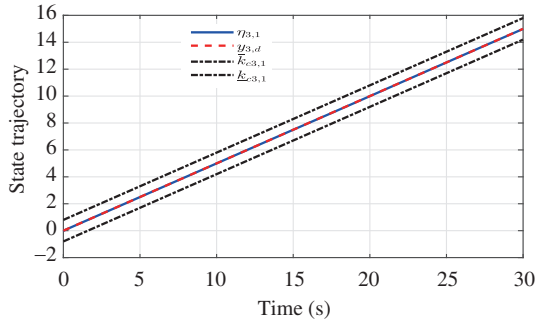

Figure 7 (Color online) The trajectories of state $\eta_{3,1}$ and desired signal $y_{3,d}$.

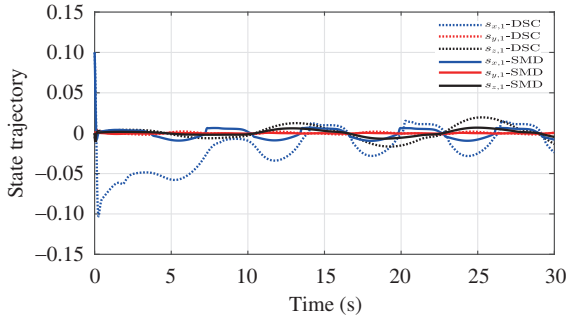

Figure 8 (Color online) The trajectories of tracking errors $s_{n,1}$.

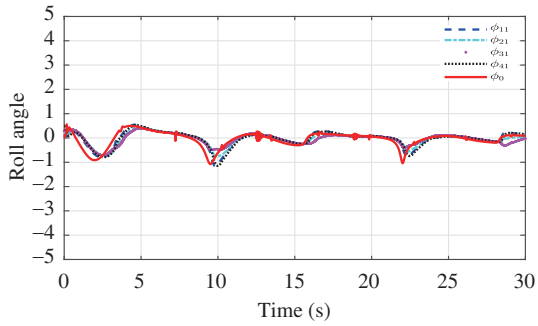

Figure 9 (Color online) The roll angle $\phi_{i,1}$ and the desired signal ϕ_0.

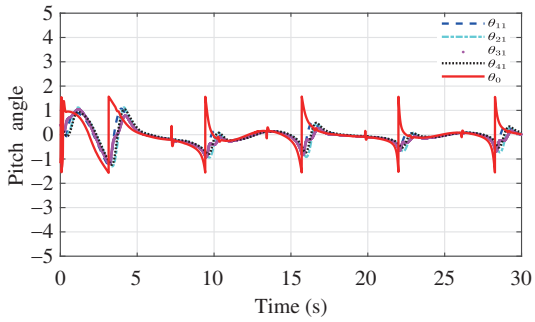

Figure 10 (Color online) The pitch angle $\theta_{i,1}$ and the desired signal θ_0.

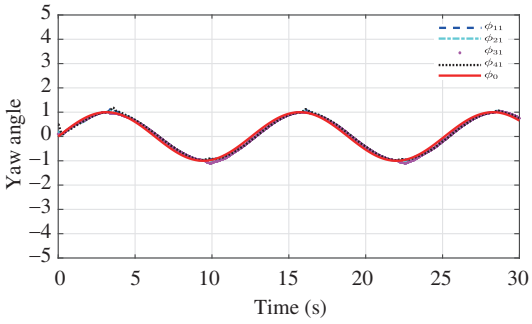

Figure 11 (Color online) The yaw angle $\psi_{i,1}$ and the desired signal ψ_0.

whereas the traditional time-triggered control method will need 30000 samples. Furthermore, to present the advantages of the proposed event-triggered strategy, three different threshold strategies are compared in Table 1. Therefore, different from the fixed threshold and switching threshold strategies, the relative threshold strategy shows the superiority in terms of mitigating unnecessary waste of network resources and actuator wear for nonlinear six-rotor UAV systems with input saturation being verified.

Remark 5. In the multi-UAV systems, the input saturation is inherent owing to the physical limitations and the energy consumption [19]. Figures 12–14 depict the responses of the actual control signal $u_{i,1}(\vartheta_{i,1})$ with saturation and the bound of $u_{i,1}(\vartheta_{i,1})$ is chosen as 40. From the simulation results, the effectiveness of the proposed control scheme has been proved for UAV systems with input saturation.

5 Conclusion

This paper has investigated the adaptive trajectory tracking control problems for nonstrict-feedback nonlinear six-rotor UAV systems with asymmetric time-varying output constraints and input saturation. In

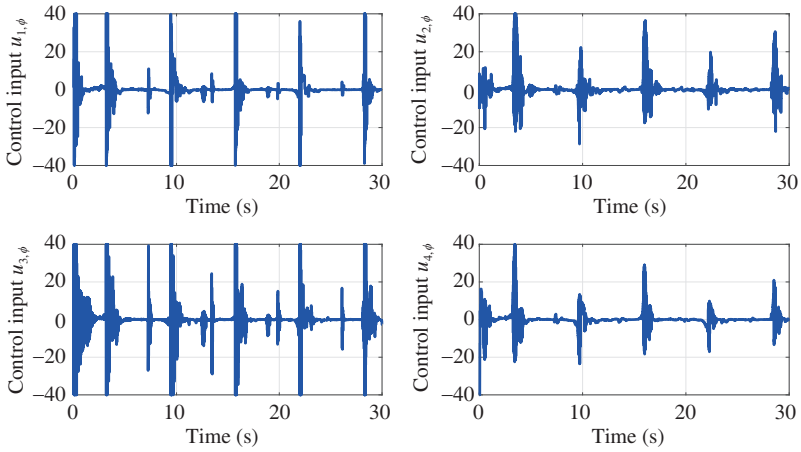

Figure 12 (Color online) The control input $u_{i,\phi}(\vartheta_i)$ of attitude systems.

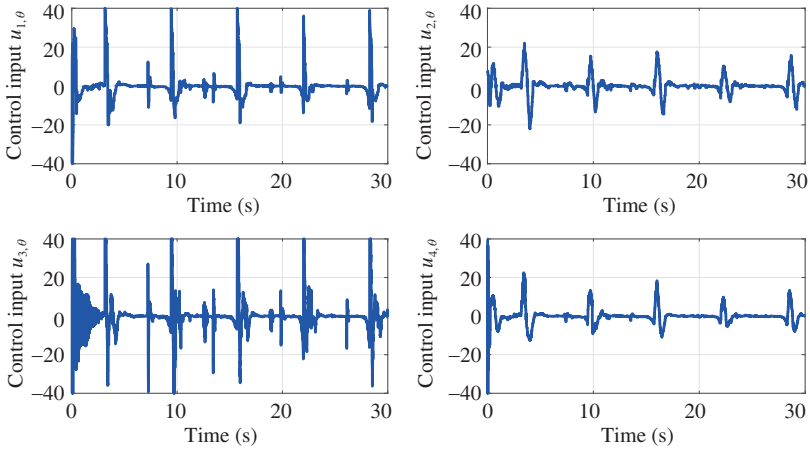

Figure 13 (Color online) The control input $u_{i,\theta}(\vartheta_i)$ of attitude systems.

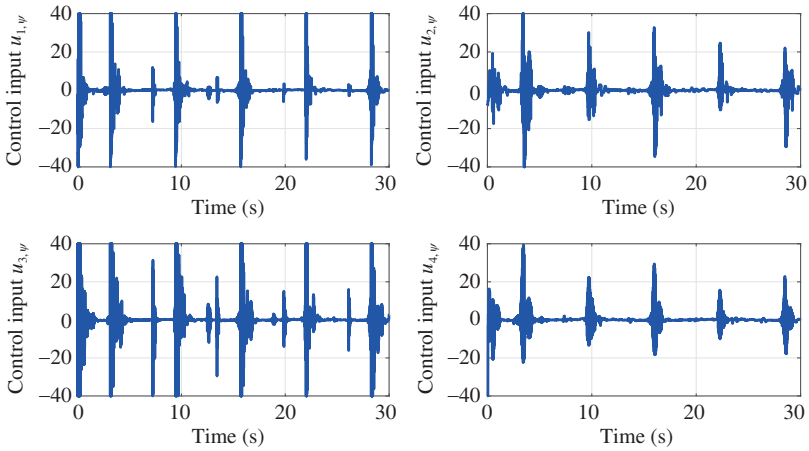

Figure 14 (Color online) The control input $u_{i,\psi}(\vartheta_i)$ of attitude systems.

the backstepping framework, the first-order SMD has been proposed to solve the"explosion of complexity" issue. By introducing the asymmetric time-varying BLF and an auxiliary function, the outputs of violating time-varying and actuator input saturation constraint have been prevented, respectively. In addition, a distributed adaptive event triggering tracking control strategy has been proposed to ensure the fast tracking of Euler angles. Based on the adjusted event triggering parameters, communication burden is alleviated by reducing the number of transmitted messages. Simulation results have validated

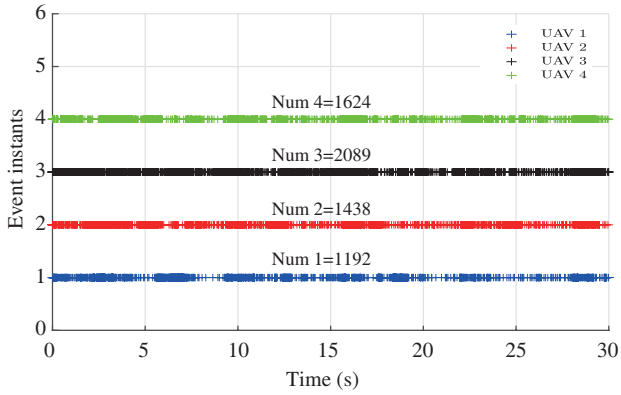

Figure 15 (Color online) Release instants of the UAV systems 1–4.

Table 1 Number of triggering events

	UAV 1	UAV 2	UAV 3	UAV 4
Fixed threshold method in [27]	4287	4081	4383	3813
Switching threshold method in [44]	1538	1694	2367	2103
Relative threshold method	1192	1438	2089	1624

the effectiveness of the proposed adaptive tracking control algorithm for six-rotor UAV systems. A significant topic for future investigation is investigating the finite time control problems for UAV systems with time-delay and failures [45–49].

Acknowledgements This work was partially supported by National Natural Science Foundation of China (Grant Nos. 62033003, 62003093, 61803105, U1911401), Local Innovative and Research Teams Project of Guangdong Special Support Program (Grant No. 2019BT02X353), China Postdoctoral Science Foundation (Grant No. 2020M682614), and Science and Technology Program of Guangzhou (Grant No. 201904020006).

References

1 Cai G W, Chen B M, Peng K, et al. Modeling and control of the yaw channel of a UAV helicopter. IEEE Trans Ind Electron, 2008, 55: 3426–3434
2 Lin F, Dong X X, Chen B M, et al. A robust real-time embedded vision system on an unmanned rotorcraft for ground target following. IEEE Trans Ind Electron, 2012, 59: 1038–1049
3 Duan H B, Xin L, Chen S J. Robust cooperative target detection for a vision-based UAVs autonomous aerial refueling platform via the contrast sensitivity mechanism of eagle's eye. IEEE Aerosp Electron Syst Mag, 2019, 34: 18–30
4 Zuo Z Y, Wang C. Adaptive trajectory tracking control of output constrained multi-rotors systems. IET Control Theor Appl, 2014, 8: 1163–1174
5 Tian B, Liu L, Lu H, et al. Multivariable finite time attitude control for quadrotor UAV: theory and experimentation. IEEE Trans Ind Electron, 2018, 65: 2567–2577
6 Zhang Z, Wang F, Guo Y, et al. Multivariable sliding mode backstepping controller design for quadrotor UAV based on disturbance observer. Sci China Inf Sci, 2018, 61: 112207
7 Zuo Z Y. Adaptive trajectory tracking control design with command filtered compensation for a quadrotor. J Vib Control, 2013, 19: 94–108
8 Islam S, Liu P X, Saddik A E. Robust control of four-rotor unmanned aerial vehicle with disturbance uncertainty. IEEE Trans Ind Electron, 2015, 62: 1563–1571
9 He T P, Liu H, Li S. Quaternion-based robust trajectory tracking control for uncertain quadrotors. Sci China Inf Sci, 2016, 59: 122902
10 Xiao B, Yin S. A new disturbance attenuation control scheme for quadrotor unmanned aerial vehicles. IEEE Trans Ind Inf, 2017, 13: 2922–2932
11 He W, Ge S S. Vibration control of a flexible string with both boundary input and output constraints. IEEE Trans Contr Syst Technol, 2015, 23: 1245–1254
12 Liu Y J, Tong S. Barrier Lyapunov functions-based adaptive control for a class of nonlinear pure-feedback systems with full state constraints. Automatica, 2016, 64: 70–75
13 Lv M, Yu W, Baldi S. The set-invariance paradigm in fuzzy adaptive DSC design of large-scale nonlinear input-constrained systems. IEEE Trans Syst Man Cybern Syst, 2021, 51: 1035–1045
14 Edalati L, Sedigh A K, Shooredeli M A, et al. Adaptive fuzzy dynamic surface control of nonlinear systems with input saturation and time-varying output constraints. Mech Syst Signal Process, 2018, 100: 311–329
15 Gilbert E, Kolmanovsky I. Nonlinear tracking control in the presence of state and control constraints: a generalized reference governor. Automatica, 2002, 38: 2063–2073
16 Zhang M, Jing X. A bioinspired dynamics-based adaptive fuzzy SMC method for half-car active suspension systems with input dead zones and saturations. IEEE Trans Cybern, 2021, 51: 1743–1755
17 Tee K P, Ren B, Ge S S. Control of nonlinear systems with time-varying output constraints. Automatica, 2011, 47: 2511–2516

18 Fu C, Hong W, Lu H, et al. Adaptive robust backstepping attitude control for a multi-rotor unmanned aerial vehicle with time-varying output constraints. Aerospace Sci Tech, 2018, 78: 593–603
19 Kuriki Y, Namerikawa T. Consensus-based cooperative formation control with collision avoidance for a multi-UAV system. In: Proceedings of American Control Conference, 2014. 2077–2082
20 Dong X, Hua Y, Zhou Y, et al. Theory and experiment on formation-containment control of multiple multirotor unmanned aerial vehicle systems. IEEE Trans Automat Sci Eng, 2019, 16: 229–240
21 Zou Y, Zhou Z, Dong X, et al. Distributed formation control for multiple vertical takeoff and landing UAVs with switching topologies. IEEE/ASME Trans Mechatron, 2018, 23: 1750–1761
22 Wang J N, Zhou Z Y, Wang C Y, et al. Cascade structure predictive observer design for consensus control with applications to UAVs formation flying. Automatica, 2020, 121: 109200
23 Zhu S Y, Liu Y, Lou Y J, et al. Stabilization of logical control networks: an event-triggered control approach. Sci China Inf Sci, 2020, 63: 112203
24 Chen Z Y, Han Q-L, Yan Y M, et al. How often should one update control and estimation: review of networked triggering techniques. Sci China Inf Sci, 2020, 63: 150201
25 Zhu W, Wang D D, Zhou Q H. Leader-following consensus of multi-agent systems via adaptive event-based control. J Syst Sci Complex, 2019, 32: 846–856
26 Su Y, Wang Q, Sun C. Self-triggered consensus control for linear multi-agent systems with input saturation. IEEE/CAA J Autom Sin, 2020, 7: 150–157
27 Yang B, Zhou Q, Cao L, et al. Event-triggered control for multi-agent systems with prescribed performance and full state constraints (in Chinese). Acta Autom Sin, 2019, 45: 1527–1535
28 Yao D, Li H, Lu R, et al. Distributed sliding-mode tracking control of second-order nonlinear multiagent systems: an event-triggered approach. IEEE Trans Cybern, 2020, 50: 3892–3902
29 Ma H, Li H Y, Lu R Q, et al. Adaptive event-triggered control for a class of nonlinear systems with periodic disturbances. Sci China Inf Sci, 2020, 63: 150212
30 Zhang H, Chen J, Wang Z P, et al. Distributed event-triggered control for cooperative output regulation of multiagent systems with an online estimation algorithm. IEEE Trans Cybern, 2020. doi: 10.1109/TCYB.2020.2991761
31 Liang H, Liu G, Zhang H, et al. Neural-network-based event-triggered adaptive control of nonaffine nonlinear multiagent systems with dynamic uncertainties. IEEE Trans Neural Netw Learning Syst, 2021, 32: 2239–2250
32 Bai W W, Chen G D, Zhou Q, et al. Disturbance-observer-based event-triggered control for multi-agent systems with input saturation (in Chinese). Sci Sin Inform, 2019, 49: 1502–1516
33 Chen F, Jiang R, Zhang K, et al. Robust backstepping sliding mode control and observer-based fault estimation for a quadrotor UAV. IEEE Trans Ind Electron, 2016, 63: 5044–5056
34 Xu B, Shi Z K, Sun F C, et al. Barrier Lyapunov function based learning control of hypersonic flight vehicle with AOA constraint and actuator faults. IEEE Trans Cybern, 2019, 49: 1047–1057
35 Chen J, Kai S X. Cooperative transportation control of multiple mobile manipulators through distributed optimization. Sci China Inf Sci, 2018, 61: 120201
36 Xu X, Liu L, Feng G. Consensus of single integrator multi-agent systems with unbounded transmission delays. J Syst Sci Complex, 2019, 32: 778–788
37 Li Z, Gao L, Chen W, et al. Distributed adaptive cooperative tracking of uncertain nonlinear fractional-order multi-agent systems. IEEE/CAA J Autom Sin, 2020, 7: 292–300
38 Lin G H, Li H Y, Ma H, et al. Human-in-the-loop consensus control for nonlinear multi-agent systems with actuator faults. IEEE/CAA J Autom Sin, 2020. doi: 10.1109/JAS.2020.1003596
39 Li H Y, Wu Y, Chen M. Adaptive fault-tolerant tracking control for discrete-time multi-agent systems via reinforcement learning algorithm. IEEE Trans Cybern, 2021, 51: 1163–1174
40 Zhou Q, Zhao S, Li H, et al. Adaptive neural network tracking control for robotic manipulators with dead zone. IEEE Trans Neural Netw Learn Syst, 2019, 30: 3611–3620
41 Xu B, Yang D P, Shi Z K, et al. Online recorded data-based composite neural control of strict-feedback systems with application to hypersonic flight dynamics. IEEE Trans Neural Netw Learn Syst, 2018, 29: 3839–3849
42 Bai W W, Li T S, Tong S C. NN reinforcement learning adaptive control for a class of nonstrict-feedback discrete-time systems. IEEE Trans Cybern, 2020, 50: 4573–4584
43 Wang F, Chen B, Lin C, et al. Distributed adaptive neural control for stochastic nonlinear multiagent systems. IEEE Trans Cybern, 2017, 47: 1795–1803
44 Xi C, Dong J. Event-triggered adaptive fuzzy distributed tracking control for uncertain nonlinear multi-agent systems. Fuzzy Sets Syst, 2021, 402: 35–50
45 Liu Y, Liu X, Jing Y, et al. Annular domain finite-time connective control for large-scale systems with expanding construction. IEEE Trans Syst Man Cybern Syst, 2020. doi: 10.1109/TSMC.2019.2960009
46 Pan Y, Du P, Xue H, et al. Singularity-free fixed-time fuzzy control for robotic systems with user-defined performance. IEEE Trans Fuzzy Syst, 2020. doi: 10.1109/TFUZZ.2020.2999746
47 Zhang C K, Long F, He Y, et al. A relaxed quadratic function negative-determination lemma and its application to time-delay systems. Automatica, 2020, 113: 108764
48 Long F, Jiang L, He Y, et al. Stability analysis of systems with time-varying delay via novel augmented Lyapunov-Krasovskii functionals and an improved integral inequality. Appl Math Comput, 2019, 357: 325–337
49 Zhang H, Wang J. Active steering actuator fault detection for an automatically-steered electric ground vehicle. IEEE Trans Veh Technol, 2017, 66: 3685–3702